Numerical analysis of vortex motion in two-dimensional array of Josephson junctions

K. Nakajima and Y. Sawada

Citation: Journal of Applied Physics **52**, 5732 (1981); doi: 10.1063/1.329514
View online: http://dx.doi.org/10.1063/1.329514
View Table of Contents: http://scitation.aip.org/content/aip/journal/jap/52/9?ver=pdfcov
Published by the AIP Publishing

Numerical analysis of vortex motion in two-dimensional array of Josephson junctions

K. Nakajima and Y. Sawada

Research Institute of Electrical Communication, Tohoku University, Sendai, Japan
(Received 9 February 1981; accepted for publication 21 May 1981)

We show that the equation which describes two- and three-dimensional arrays of small-area Josephson junctions is reduced to the following form, $-\nabla\times(\nabla\times\Phi)-\partial^2\Phi/\partial t^2-\Gamma\partial\Phi/\partial t=\sin\Phi$, where Φ is the two- or three-dimensional phase-difference vector, and $\sin\Phi$ is the vector whose components are sine functions of the components of Φ, respectively. Based on the above equation we analyze numerically a two-dimensional square network of Josephson junctions, and discuss the vortex motion on the network.

PACS numbers: 74.50. + r

I. INTRODUCTION

Josephson devices combine high-speed with low-power dissipation, which makes them attractive elements for high-performance computer circuits.[1] It is now possible to make Josephson integrated circuits with reasonable mechanical and electrical stability.[2] In previous papers[3,4] we proposed a Josephson computing network using continuous or discrete Josephson-junction transmission lines which are described by the sine-Gordon equation having a loss term and a bias term. Moreover, research in recent years exhibits an increase of interest in distributed Josephson logic devices where the principle of operation is based on the known properties of isolated fluxoids.[5,6]

In the present paper we discuss the vortex motion in a two-dimensional array of small-area Josephson junctions. This type of Josephson network is expected to have all logic functions which we have reported in our previous papers,[3,4] and also is expected to show the kinetic momentum quantum effect.[7] Because it is easy to fabricate, as its arrangement is very simple, two-dimensional array of small-area Josephson junctions is suitable for the integrated circuit of a high-performance computer. This type of circuit was also investigated for microwave application.[8] In Sec. II we describe a differential-difference equation of a two-dimensional array of small-area Josephson junctions and its equivalent circuit. This equation is reduced to a partial differential equation describing a vector field by extending it to continuous variables. We are interested in the two-dimensional solitary wave solution of this vector field and in the relation of this network and a type-II superconductor. Section III deals with numerical analyses of a square network of Josephson junctions based on the equation derived in Sec. II. We discuss distribution of magnetic field, one vortex solution, the interaction of two fluxoids, and the active propagation of a single fluxoid. Section IV is the conclusion.

II. TWO-DIMENSIONAL ARRAY OF JOSEPHSON JUNCTIONS

Let us consider a square array of superconductors whose up side, down side, left side, and right side are connected by Josephson junctions, respectively, as shown in Fig. 1. We assume the junctions are small enough that they never contain an appreciable fraction of flux quantum, and the superconductors are large enough for magnetic flux never to penetrate beyond penetration depth.

Each junction's phase parameter[9,10] is designated by three parameters (x,i,j) or (y,i,j), as shown in Fig. 1. The phase parameter for which junction plane is perpendicular to the x co-ordinate is represented as ϕ_x, and another is represented as ϕ_y. The following relation is given between phase parameters,[10]

$$\begin{aligned}&\phi_y(i+1,j)-\phi_x(i,j+1)-\phi_y(i,j)+\phi_x(i,j)\\&=\left[\theta_2-\theta_1-\left(\frac{2e}{\hbar}\right)\int_1^2 A_y\,dy\right]-\left[\theta_3-\theta_4-\left(\frac{2e}{\hbar}\right)\int_4^3 A_x\,dx\right]-\left[\theta_5-\theta_6-\left(\frac{2e}{\hbar}\right)\int_6^5 A_y\,dy\right]+\left[\theta_8-\theta_7-\left(\frac{2e}{\hbar}\right)\int_7^8 A_x\,dx\right]\\&=-\int_2^3\nabla\theta\,d\mathbf{l}-\int_4^5\nabla\theta\,d\mathbf{l}-\int_6^7\nabla\theta\,d\mathbf{l}-\int_8^1\nabla\theta\,d\mathbf{l}-\left(\frac{2e}{\hbar}\right)\left(\int_1^2 A_y\,dy+\int_3^4 A_x\,dx+\int_5^6 A_y\,dy+\int_7^8 A_x\,dx\right)=-(2e/\hbar)\oint\mathbf{A}\,d\mathbf{l}\,,\end{aligned}\tag{1}$$

because supercurrent $\mathbf{J}_s=0$ in superconductors, so $\nabla\theta=(2e/\hbar)\mathbf{A}$, where θ's are phases of superconductors, $\mathbf{A}$ is a vector potential, and $\mathbf{l}$ is the integration contour shown in Fig. 1. Equation (1) can be written as,

$$\phi_y(i+1,j)-\phi_x(i,j+1)-\phi_y(i,j)+\phi_x(i,j)=-(2e/\hbar)\,S\mu_0 H_z(i,j)\,,\tag{2}$$

where S is the area inside the loop, $H_z(i,j)$ is the average magnetic field inside the loop, and we assume the existence of only the Z component of the magnetic field. From the surface integral of Maxwell's first equation and

 0021-8979/81/095732-12$01.10

$E(i,j)d=(\hbar/2e)\,\partial\phi(i,j)/\partial t$, where E is an electric field inside a barrier perpendicular to it, and d is the barrier thickness, we have

$$-a[H_z(i,j)-H_z(i-1,j)]=(\hbar/2e)(\epsilon s/d)\partial^2\phi_y(i,j)/\partial t^2+(\hbar/2e)(\sigma s/d)\partial\phi_y(i,j)/\partial t+sJ_c\sin\phi_y(i,j)\,, \tag{3}$$

$$a[H_z(i,j)-H_z(i,j-1)]=(\hbar/2e)(\epsilon s/d)\partial^2\phi_x(i,j)/\partial t^2+(\hbar/2e)(\sigma s/d)\partial\phi_x(i,j)/\partial t+sJ_c\sin\phi_x(i,j)\,, \tag{4}$$

where we assume that all junctions have the same characteristics. a is the width of junction in the Z direction, ϵ is the dielectric constant of the barrier, s is the area of junction, σ is the conductivity of the barrier, and J_c is the critical current density. From Eqs. (2)–(4) we obtain a differential-difference equation, and it can be written for the three-dimensional network in the following vector form, for simplicity,

$$-(\hbar/2e)[(1/L)\nabla'\times(\nabla'\times\Phi)+C\partial^2\Phi/\partial t^2+G\partial\Phi/\partial t]=I_c\sin\Phi\,, \tag{5}$$

$$\Phi=\begin{bmatrix}\phi_x(i,j,k)\\ \phi_y(i,j,k)\\ \phi_z(i,j,k)\end{bmatrix}\,, \tag{6}$$

$$\sin\Phi=\begin{bmatrix}\sin\phi_x(i,j,k)\\ \sin\phi_y(i,j,k)\\ \sin\phi_z(i,j,k)\end{bmatrix}\,, \tag{7}$$

$$\nabla'\times\Phi=\begin{vmatrix}\mathbf{i}&\mathbf{j}&\mathbf{k}\\ \Delta_x&\Delta_y&\Delta_z\\ \phi_x&\phi_y&\phi_z\end{vmatrix}\,, \tag{8}$$

where $L=\mu_0 S/a$, $C=\epsilon s/d$, $G=\sigma s/d$, $I_c=sJ_c$, and i, j, k are unit vectors of x, y, z components, respectively. Δ_x, Δ_y, and Δ_z are finite difference operators. If $\phi_x(i,j,k)=\phi_x(i,j)$, $\phi_y(i,j,k)=\phi_y(i,j)$, $\phi_z(i,j,k)=0$, and $\Delta_z=0$ in Eq. (5), we get the two-dimensional form which are the same equations as the equations obtained from Eqs. (2)–(4). If we consider a limiting case $\Delta 1\to 0$, Eq. (5) is reduced to a partial differential equation for a vector field, and the operator $\nabla'\times$ is reduced to the usual differential operator $\nabla\times$. Equation (5) can be transformed to the same equation as Eq. (4) of Ref. 4 which represents a discrete Josephson junction transmission line. If we leave only the y component in Eq. (5), namely, $\phi_x(i,j,k)=0$, $\phi_y(i,j,k)=\phi_i$, $\phi_z(i,j,k)=0$, $\Delta_y=0$, and $\Delta_z=0$, we can obtain Eq. (4) of Ref. 4, and under the condition of $\Delta x\to 0$ the equation is reduced to the sine-Gordon equation with loss term. The equivalent circuit of the two-dimensional array of the Josephson junctions, which corresponds to Fig. 1, namely Eq. (5), is shown in Fig. 2. In the equivalent circuit, Josephson junctions are connected to each other by loop inductance, and no loop current flows in the loop inductance as shown in Fig. 2, because the loop inductance represents a superconductor, and no magnetic flux exists inside the superconductor. The following relations are given in Fig. 2:

$$I(i,j)-I(i-1,j)=(\hbar/2e)(C\partial^2\phi_y/\partial t^2+G\partial\phi_y/\partial t)+I_c\sin\phi_y(i,j)\,, \tag{9}$$

$$I(i,j-1)-I(i,j)=(\hbar/2e)(C\partial^2\phi_x/\partial t^2+G\partial\phi_x/\partial t)+I_c\sin\phi_x(i,j)\,, \tag{10}$$

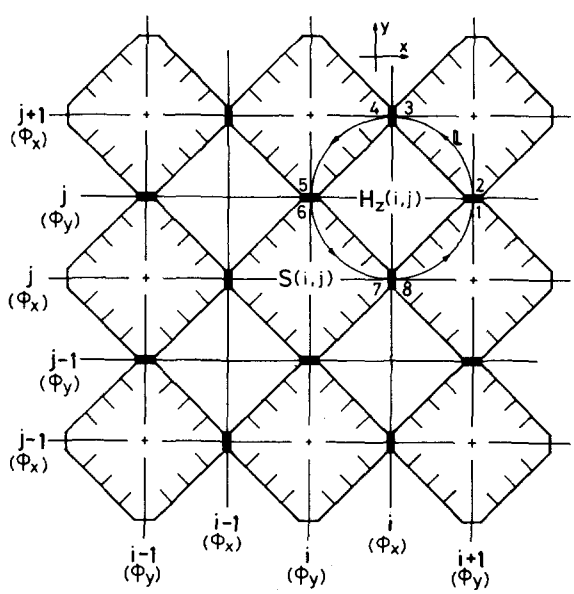

FIG. 1. Two-dimensional array of Josephson junction. $S(i,j)$ denotes a superconductor, $H_z(i,j)$ denotes a magnetic field in the direction to the Z axis. Each junction is designated by three parameters (x,i,j) or (y,i,j), and I is the integration contour.

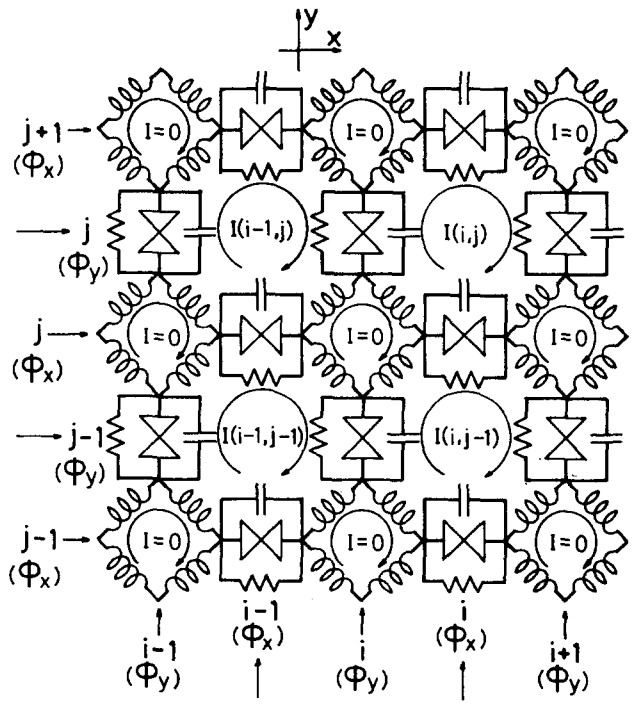

FIG. 2. Equivalent circuit of the two-dimensional array of the Josephson junctions.

and the phase parameters are restricted by the usual constraint,

$$\phi_y(i,j)+\phi_x(i,j+1)-\phi_y(i+1,j)-\phi_x(i,j) = -(2e/\hbar)LI(i,j)\ , \quad (11)$$

where L is the loop inductance in Fig. 2. We can again obtain Eq. (5) from Eqs. (9)–(11). We could construct a three-dimensional equivalent circuit, and we should get the three-dimensional form of Eq. (5) by using the same type equations as Eqs. (9)–(11). Solitary wave solution of Eq. (5) in the three-dimensional case would be interesting, but it is a future subject.

III. NUMERICAL ANALYSIS AND DISCUSSION

For simplicity, Eq. (5) is normalized as the following,

$$-(1/HL)\nabla'\times\nabla'\times\Phi-\partial^2\Phi/\partial t^2-\Gamma\partial\Phi/\partial t=\sin\Phi\ , \quad (12)$$

where time is measured in units of $\tau_J=(C\hbar/2eI_c)^{1/2}$, $HL=2eLI_c/\hbar$, and $\Gamma=G(\hbar/2eI_cC)^{1/2}$. In the following calculations for the two-dimensional form we use the normalized form of the magnetic field as

$$h_z(i,j)=aH_z(i,j)/I_c=[-\phi_y(i+1,j)+\phi_y(i,j)+\phi_x(i,j+1)-\phi_x(i,j)]/HL\ . \quad (13)$$

And we use the same finite-difference method as Ref. 11 for the numerical calculation of Eq. (12). Our model of square network, where $\Gamma=$ const and the small increment of time $\Delta t=0.1(HL)^{1/2}$ are assumed, is constructed of a two-dimensional array of 31×31 superconductors, so $\phi_x(i_{max},j_{max})=\phi_x(30,31)$, $\phi_y(i_{max},j_{max})=\phi_y(31,30)$, and $h_z(i_{max},j_{max})=h_z(30,30)$. The results of computer simulation would be summarized as follows.

A. Effect of external magnetic field

Figure 3 shows h_z of the square network which is in a Meissner state when the external field h_a is applied under the condition of $h_a=5.0$, and $HL=0.1$. When the external field is applied, the boundary condition is given from Eqs. (3) and (4). h_z has the largest value ~4.54 at the four corners of the square network. The value of h_z decreases with the distance from the edge of the square network. Let us estimate the decreasing rate of h_z. When the time derivative terms are neglected from Eq. (12), and the limiting case is assumed, we have

$$\partial^2\phi_x/\partial y^2-\partial^2\phi_y/\partial y\partial x=\mathcal{L}\sin\phi_x\ , \quad (14)$$

and

$$\partial^2\phi_y/\partial x^2-\partial^2\phi_x/\partial x\partial y=\mathcal{L}\sin\phi_y\ . \quad (15)$$

where $\mathcal{L}=HL/S$ and $S=\Delta1^2$. If we assume that the network lies in a half plane ($x>0$), and that the external field is directed along the z axis, it is considered that the supercurrent flows in the direction of the y axis only. In this case $\phi_x=0$ and ϕ_y is the function of x only, so Eqs. (14) and (15) become

$$\partial^2\phi_y/\partial x^2=\mathcal{L}\sin\phi_y\ , \quad (16)$$

while h_z becomes the following form from Eq. (13) under the condition of $\Delta x\to0$,

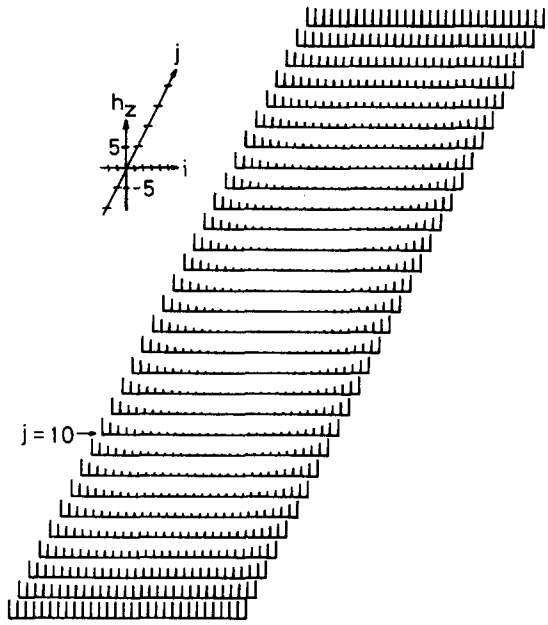

FIG. 3. Numerically obtained normalized field of the square network. External field $h_a=5.0$, and $HL=0.1$.

$$h_z=-(\Delta x/HL)\partial\phi_y/\partial x\ . \quad (17)$$

Therefore the penetration depth of h_z is $(1/\mathcal{L})^{1/2}$ which corresponds to the Josephson penetration depth. Figure 4 shows ϕ_y and ϕ_x of the square network under the same condition as Fig. 3. It can be seen from Fig. 4 that ϕ_y has a positive value at the left-side edge, and then it decreases with the distance from the edge, and that it has a negative value at the right-side edge, and that the value of ϕ_y is nearly zero at both the up and down side. While ϕ_x has a positive value at the up-side edge, and a negative value at the down-side edge, it is nearly equal to zero at both the left and right side. According to Eq. (16) the absolute value of ϕ_y decreases with the distance from the left- or right-side edge, because the condition, which is assumed when Eq. (16) is derived, is satisfied about the center of both the left- and right-side edge. It is reasonable from Eq. (17) that ϕ_y has an opposite sign at the left- and right-side edge. We can obtain the values of $\sin\phi_y$ and $\sin\phi_x$ from ϕ_y and ϕ_x shown in Fig. 4. It can be seen from them that the circulating supercurrent flows along the edge of square network, and that the circulating current induces a magnetic flux opposite to the applied magnetic field. Therefore the circulating current is a diamagnetic current, and the square network itself is equivalent to a superconductor. In the next step of computer simulation we increase abruptly the external magnetic field h_a from $h_a=5.0$ to $h_a=6.0$. Then magnetic flux penetrates into the network, and distributes under the condition of $h_a=6.0$, as is shown in Fig. 5(a). Figure 5(a) shows h_z of the network which is in a mixed state. It can be seen from Fig. 5(a) that the distribution of magnetic flux is not symmetrical. The reason seems to be that magnetic flux has to be quantized in the network, and a quantized flux has to pass through the junction located at the edge of the network to penetrate into the network. Each junction seems to have nearly same proba-

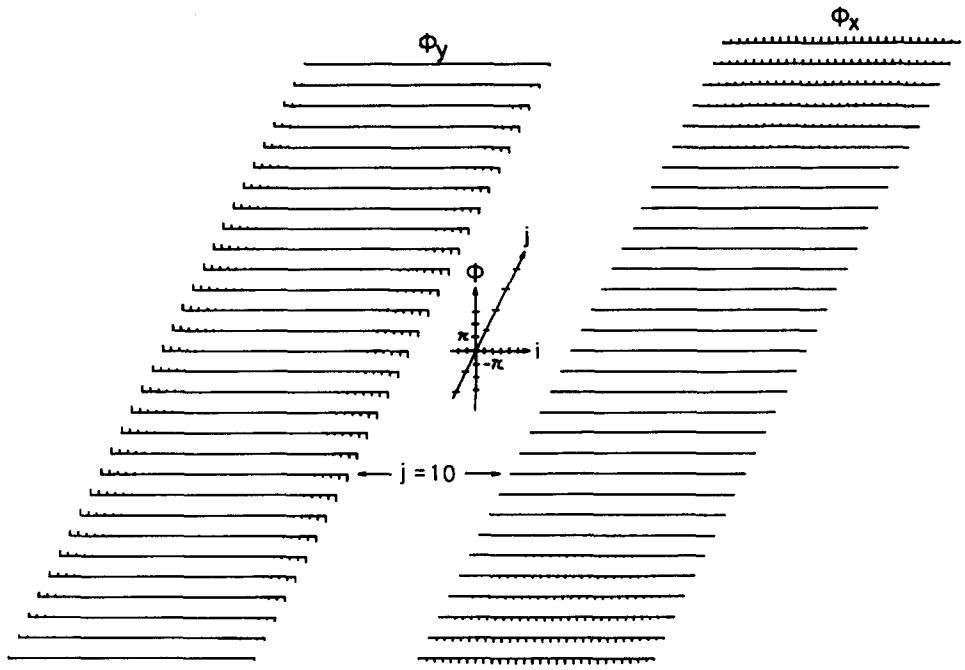

FIG. 4. Numerically obtained phase parameter of the square network under the same condition as Fig. 3.

bility to pass a quantized flux, but all junctions cannot pass a quantized flux under the restriction of a external field, therefore the selection of the junction is carried out. It seems that this condition is sensitive to noise because of the marginal state of the junction, so the selection is done depending on noise. In Fig. 5(a) h_z is relatively small at the center of the network, so it seems that some pinning forces act on the flux. The nonlinearity of $\sin\phi$ and the discreteness of the network seem to cause the pinning forces. When we take off the external field abruptly from the above situation, some quantized fluxes are left trapped in the network, which is shown in Fig. 5(b). It can be seen from Fig. 5(b) that there are some pinning forces.

B. One vortex solution (fluxoid)

We will discuss a one vortex (fluxoid) solution in the network. A one vortex solution in a superconducting closed loop composed of four Josephson junctions has been discussed by using a mechanical analog in Ref. 7. This solution is shown in Fig. 6(a) where the loop inductance is neglected for simplicity, and θ denotes the phase of the order parameter, and $\phi_{y1} = \theta_4 - \theta_1$, $\phi_{y2} = \theta_3 - \theta_2$, $\phi_{x1} = \theta_2 - \theta_1$, $\phi_{x2} = \theta_3 - \theta_4$. Therefore Eq. (11) is satisfied in Fig. 6(a), and that the circulating supercurrent $I = I_c \sin\phi$ flows as shown in Fig. 6(a). From Fig. 6(a) we can estimate the value of θ around the vortex in the square network which is shown in Fig. 6(b).

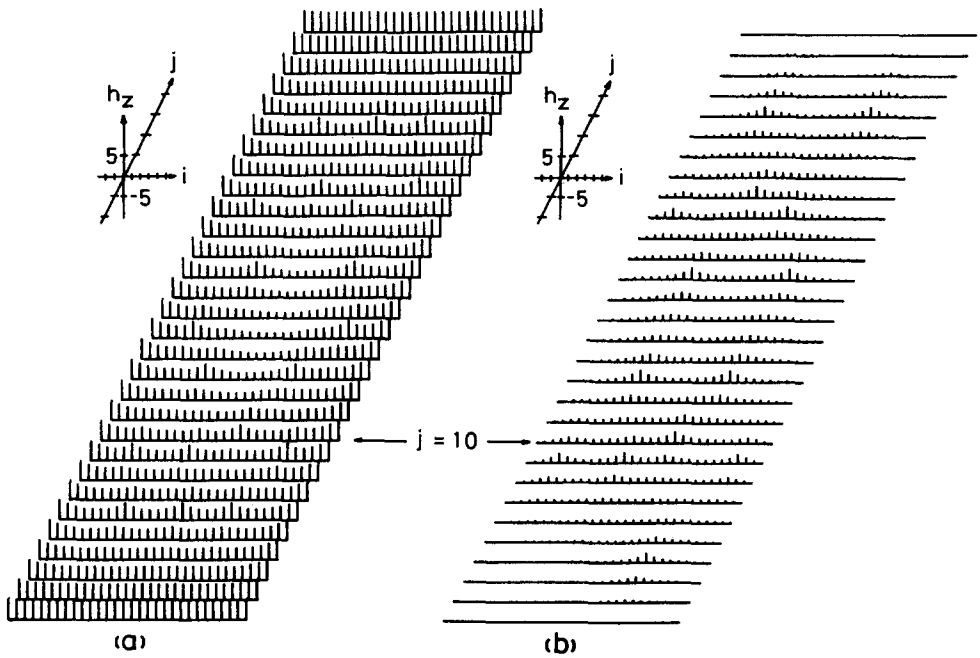

FIG. 5. Numerically obtained normalized field of the square network. (a) External field $h_a = 6.0$. (b) External field $h_a = 0$ which was taken off abruptly from $h_a = 6.0$ in the case of (a).

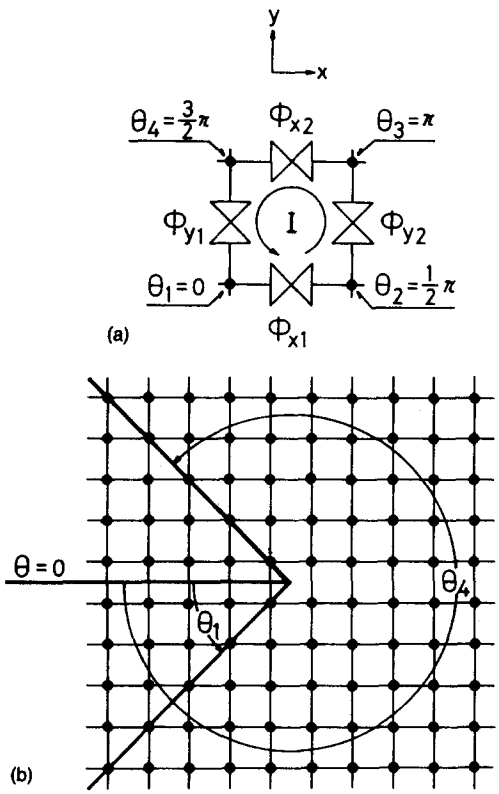

FIG. 6. (a) A one-vortex solution in a superconducting closed loop composed of four Josephson junctions: $\phi_{y1}=\theta_4-\theta_1$, $\phi_{y2}=\theta_3-\theta_2$, $\phi_{x1}=\theta_2-\theta_1$, and $\phi_{x2}=\theta_3-\theta_4$. (b) An estimation of the phase of the order parameter around the vortex in the square network.

One can add a constant to the value of the phase, so θ_1 and θ_4 in Fig. 6(b) are equal to θ_1 and θ_4 in Fig. 6(a), respectively. When the origin of the polar coordinate (r, ψ) is fixed at the center of the vortex, the value of ψ is equal to that of the phase θ of the order parameter. This characteristic is popular, and the cut of $\theta=0$ shown in Fig. 6(b) is considered to represent the trace through which the vortex center has passed. We can estimate the value of ϕ in the network from the obtained value of θ. But the value of ϕ which is obtained from the difference between the neighboring θ's is not precise because of the neglect of the loop inductance. So we use the value of ϕ obtained in this way as an initial value to calculate a one-vortex solution numerically. Figures 7(a) and 7(b) show the obtained one-vortex solution under the condition of $HL=0.1$, where the center of the vortex is between $\phi_y(15, 15)$ and $\phi_y(16.15)$, and between $\phi_x(15, 15)$ and $\phi_x(15, 16)$. The shape of the solution ϕ_y on the line $j=15$ is similar to the one-soliton solution of the sine-Gordon equation. The values of $\phi_y(1 \leqq i \leqq 15, j)$'s are negative except for $j=15$, while those of $\phi_y(16 \leqq i \leqq 31, j)$'s are positive. The values of $\phi_x(i, 1 \leqq j \leqq 15)$'s are positive, while those of $\phi_x(i, 16 \leqq j \leqq 31)$'s are negative. These results are consistent with the estimation of Fig. 6(b). Figures 7(c), 7(d), and 7(e) show h_z and $\sin\phi$ of the one-vortex solution which are obtained from Figs. 7(a) and 7(b). h_z is localized around the center of the vortex, and has the maximum value of $h_z(15, 15) \simeq 2.34$ at the center of the vortex, as is shown in Fig. 7(c). It can be seen from Figs. 7(d) and 7(e) that the loop current flows around the center of

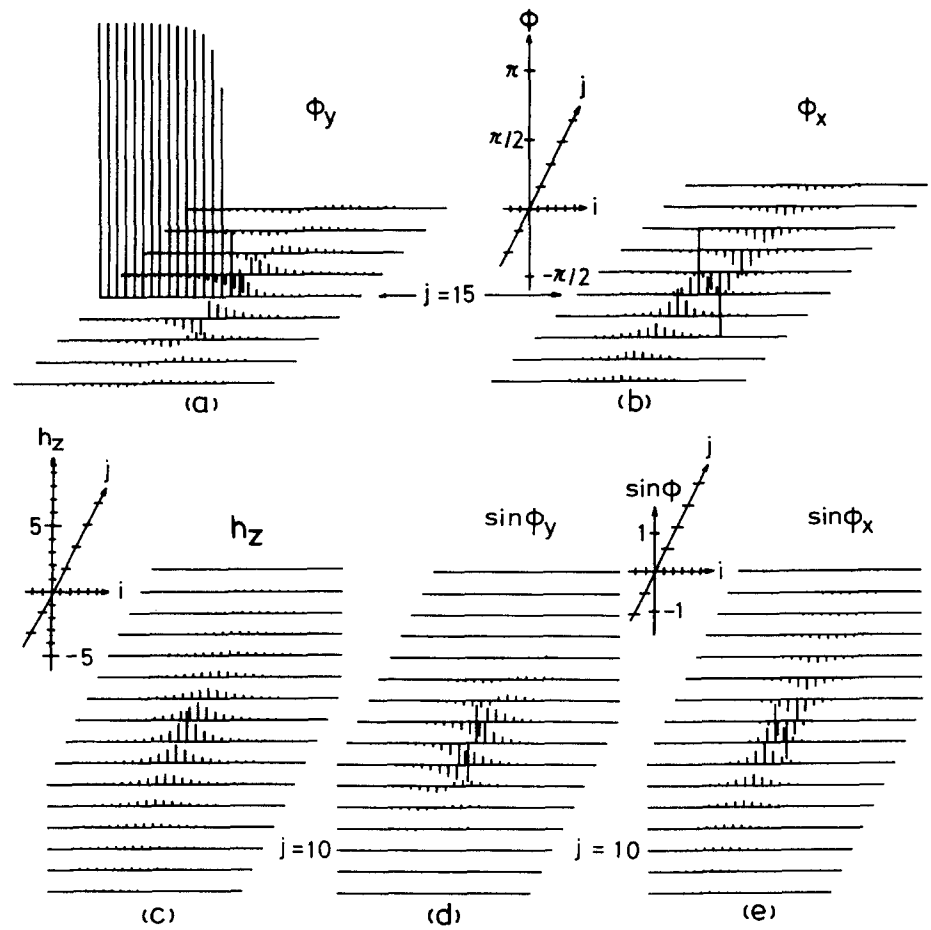

FIG. 7. (a) and (b) represent a numerically obtained single-vortex solution under the condition of $HL=0.1$. (c) is a normalized field and (d) and (e) are Josephson currents of the single-vortex solution which was obtained from (a) and (b).

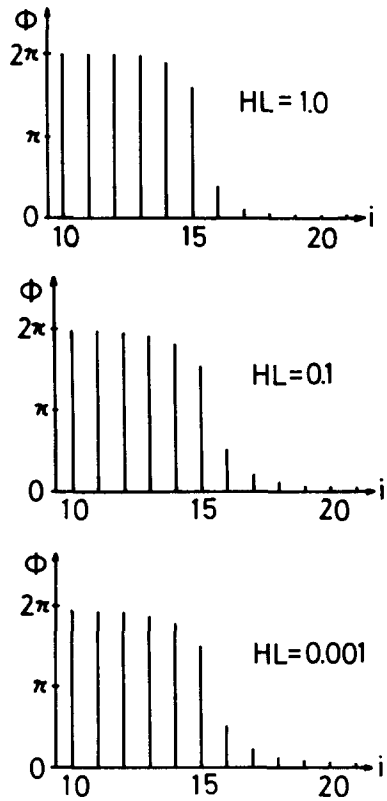

FIG. 8. Some phase parameter values around the center of a single-vortex solution for various values of HL.

vortex in a direction to keep the flux shown in Fig. 7(c), where $-\sin\phi_y(15,15)$, $\sin\phi_y(16,15)$, $\sin\phi_x(15,15)$, and $-\sin\phi_x(15,16)$ all have the same value of ~ 0.998. Next we shall investigate the kinetic momentum quantum effect.[7] Figure 8 shows the value of $\phi_y(i=10\sim21, j=15)$ for three values of HL when the network sustains a vortex whose center is between $\phi_y(15,15)$ and $\phi_y(16,15)$, and between $\phi_x(15,15)$ and $\phi_x(16,15)$. Figure 8 suggests that the shape of the solution hardly depends on the value of HL. The differences between $\phi_y(15,15)$ and $\phi_y(16,15)$ are $0.61\times2\pi$, $0.52\times2\pi$, and $0.50\times2\pi$ for $HL=1.0$, 0.1, and 0.001, respectively. The differences between $\phi_y(14,15)$ and $\phi_y(17,15)$ are $0.90\times2\pi$, $0.80\times2\pi$, and $0.77\times2\pi$, for $HL=1.0$, 0.1, and 0.001, respectively. We may roughly say that 80% of the vortex is stuffed into the three sections for $HL=0.1$, and 77% of vortex is stuffed into the same sections for $HL=0.001$, and that the unit length for $HL=0.001$ is one-tenth of that for $HL=0.1$. The values of $h_z(15,15)$ obtained from the numerical calculation are 1.38, 2.34, and 34.3 for $HL=1.0$, 0.1, and 0.001, respectively. The magnetic flux in one section is proportional to $h_z \cdot HL$, so that in the section of $h_z(15,15)$ that is 1.38 for $HL=1.0$, and 0.234 for $HL=0.1$, and 0.0343 for $HL=0.001$. These results indicate the advantage of using the effective inductance of the Josephson junction in making a small-size Josephson logic circuit.

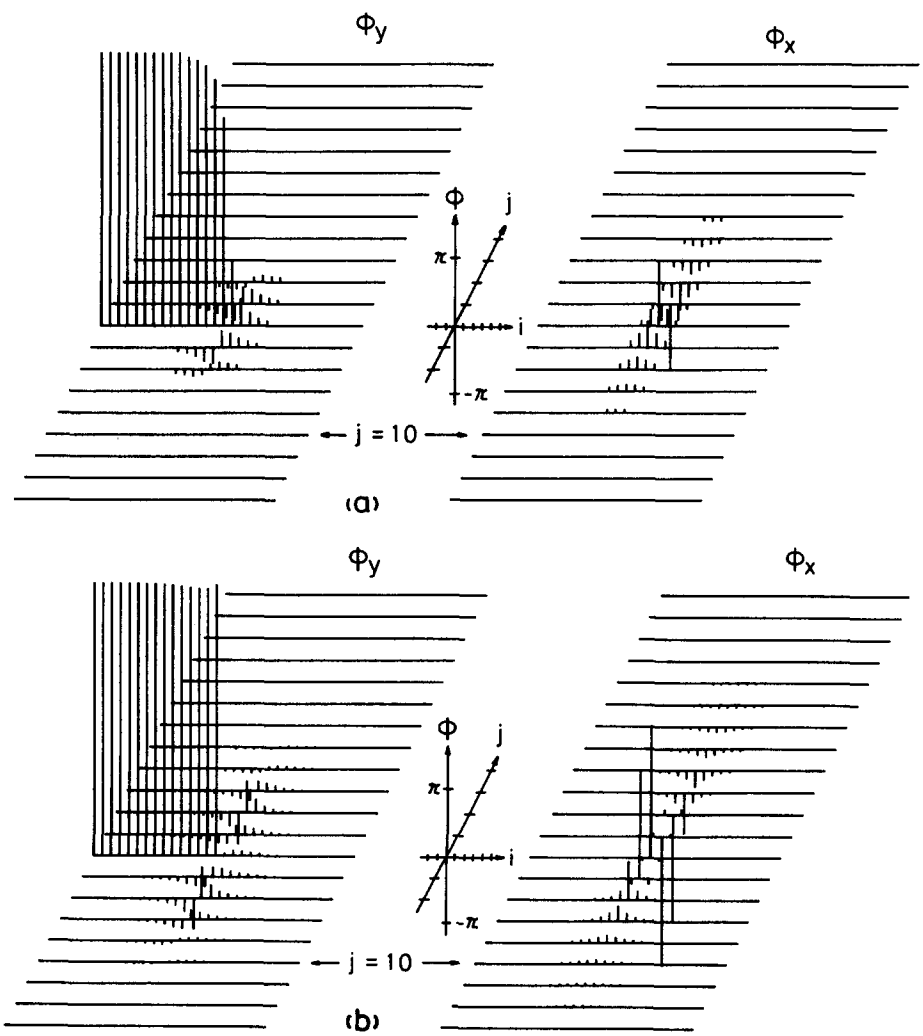

FIG. 9. Interaction of two fluxoids with the same sign. (a) Initial value of phase parameter for the numerical calculation. (b) Result after 2000 times numerical iteration.

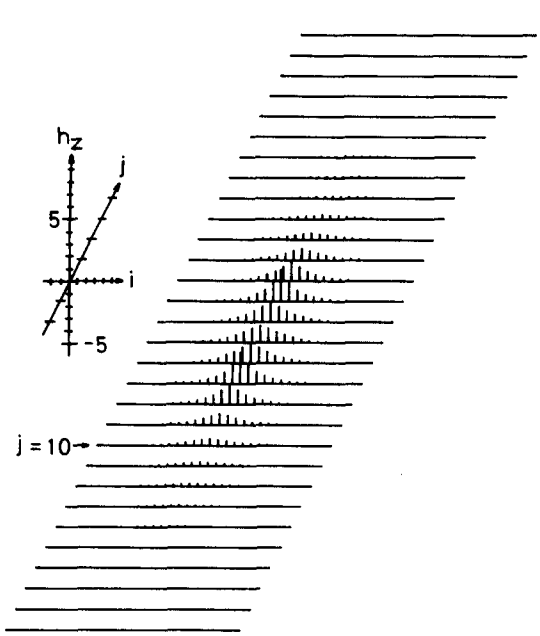

FIG. 10. Numerically obtained normalized field which was obtained from Fig. 9(b).

C. Interaction of two fluxoids

In order to investigate the dynamic behavior of the interaction of two fluxoids numerically, we chose the parameters $HL = 0.1$ and $\Gamma = 0.1$ in Eq. (12). The two fluxoids with same sign are set to overlap in the network, adding the double value of the single vortex as the initial value of the numerical calculation which is shown in Fig. 9(a). The result after 2000 times numerical iteration is shown in Fig. 9(b). The centers of two fluxoids which were set initially in the section of $h_z(15, 15)$ have repelled each other in the direction of the y axis. Figure 9(b) shows the small oscillations in the phase parameter, but the distance between the two centers of fluxoids spreads no more, and the small oscillations decrease with time according to the effect of Γ. Figure 10 shows the values of h_z which are obtained from Fig. 9(b). It can be seen from Fig. 10 that the centers of the two fluxoids have repelled each other, and they stand at the sections of $h_z(15, 13)$ and $h_z(15, 17)$, respectively. These results show that the repulsive force acts between two fluxoids with same sign as the sine-Gordon solitons, and that the pinning force acts also on the fluxoids. Figure 11 shows the result of a

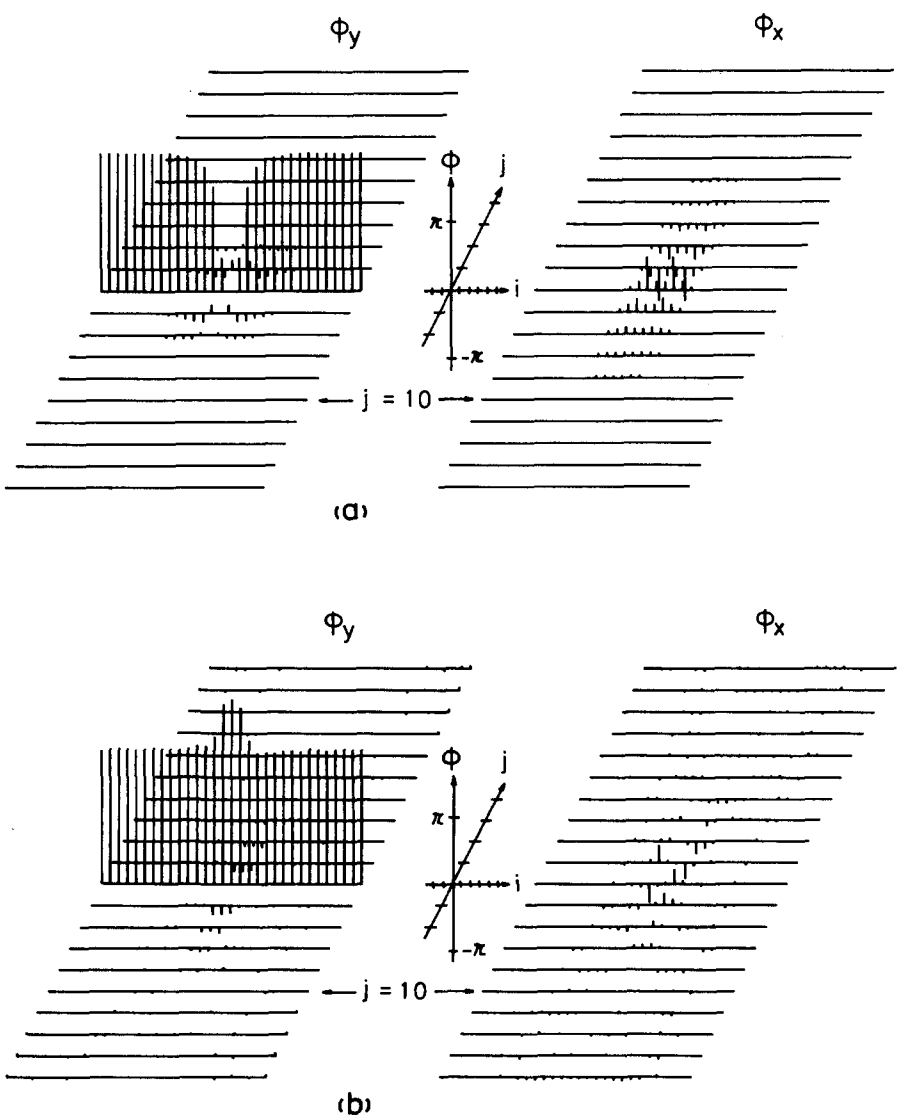

FIG. 11. Interaction of two fluxoids with opposite signs. (a) Initial value of phase parameter for the numerical calculation. (b) Result after 200 times numerical iteration.

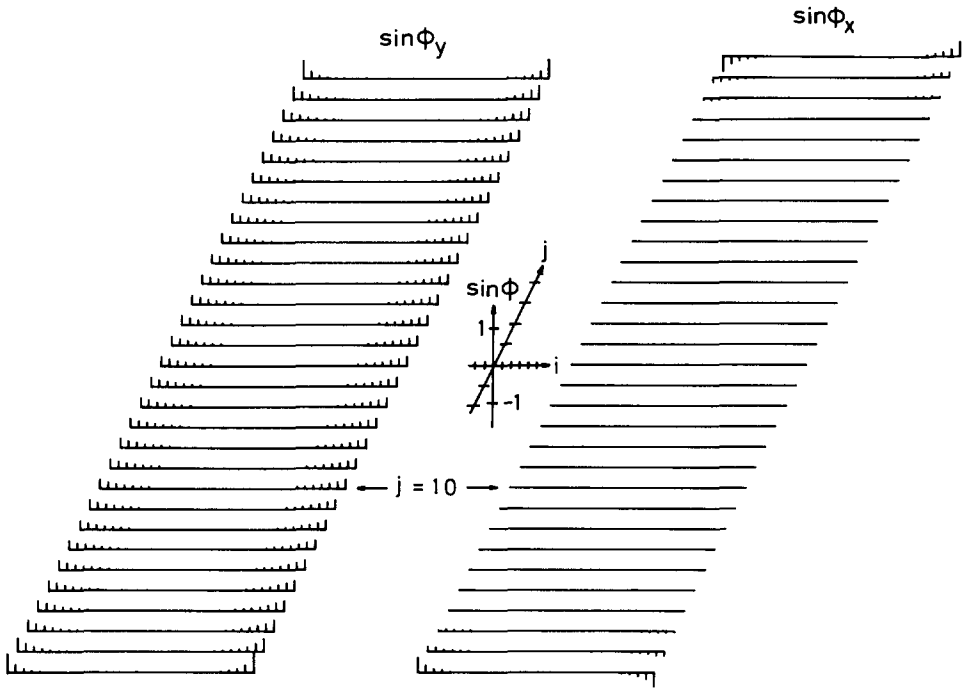

FIG. 12. Numerically obtained Josephson current distribution of the network where external currents are applied to the left- and right-side edge of the network in the direction of the y axis, that is γ_y $(1,\ j=1\sim30)=\gamma_y$ $(31,\ j=1\sim30)$ $=0.9$, another $\gamma=0$.

computer simulation which demonstrates the interaction of two fluxoids with opposite signs. Figure 11(a) shows the initial values of the phase parameters where the centers of fluxoid and antifluxoid are statically set in the sections of $h_x(14,15)$ and $h_x(17,15)$, respectively. The result after 200 times numerical iteration is shown in Fig. 11(b), where the fluxoid and the anti-fluxoid collide with each other. This result shows that there is an attractive interaction between the fluxoid and the anti-fluxoid. The small oscillation shown in Fig. 11(b) decreases with time according to the effect of Γ, and that all values of the phase parameters become equal to zero except for $\phi_y(i=1\sim31,15)$ which become 2π. Therefore the two fluxoid annihilate each other, and only a trace of the centers of the fluxoids is left on the phase parameter plane, but practically the state of the network is equal to what it was before the introduction of the two fluxoids. If the two fluxoids have kinetic energies initially, the two fluxoids seem to pass through each other as in the case of the sine-Gordon solitons.

D. Active propagation of fluxoid

One can apply external currents to the network as a Josephson transmission line. External currents I_B may be represented to add a constant term to Eq. (12) as the following,

$$-(1/HL)\nabla'\times\nabla'\times\Phi-\partial^2\Phi/\partial t^2-\Gamma\partial\Phi/\partial t=\sin\Phi-\boldsymbol{\gamma}\,, \qquad (18)$$

where

$$\boldsymbol{\gamma}=\begin{bmatrix}\gamma_x(i,\ j,\ k)\\ \gamma_y(i,\ j,\ k)\\ \gamma_z(i,\ j,\ k)\end{bmatrix},$$

$$\gamma_x=I_{Bx}/I_c\,,\quad \gamma_y=I_{By}/I_c\,,\quad \gamma_z=I_{Bz}/I_c\,,$$

and for the two-dimensional case $\gamma_x(i,j,k)=\gamma_x(i,j)$, $\gamma_y(i,j,k)=\gamma_y(i,j)$, $\gamma_z(i,j,k)=0$. Figure 12 shows the numerical result of the network where external currents are applied to the left- and right-side edge of the network in the direction of the y axis, that is $\gamma_y(1,j=1\sim30)=\gamma_y(31,j=1\sim30)=0.9$, other $\gamma_y=0$, and all $\gamma_x=0$. $\sin\phi_y$ has the largest value (~0.49) at the four corners of the square network, and the absolute value of $\sin\phi_x$ also has the largest value (~0.41) at the four corners of the square network. About the middle of the left- and right-side edges, the current vector is almost directed in the y direction. The current decreases with the distance from the side edges.

An isolated fluxoid can be driven actively by the interaction force with the external applied current. We discuss the active propagation of an isolated fluxoid in the square network represented by Eq. (18) where $HL=0.1$, $\Gamma=0.1$. Figure 13(a) shows the initial values of phase parameters where the center of the fluxoid is set between the sections $\phi_y(6,15)$ and $\phi_y(7,15)$, and between the sections $\phi_x(6,15)$ and $\phi_x(6,16)$, and the bias currents are applied as $\gamma_y(i=1\sim31,15)=0.5$, and other $\gamma=0$. The result after 1000 times numerical iteration is shown in Fig. 13(b). The center of the fluxoid reaches between the sections $\phi_y(21,15)$ and $\phi_y(22,15)$, and between the sections $\phi_x(21,15)$ and $\phi_x(21,16)$. Figure 13(b) shows that the small oscillations of phase parameters occur with the propagation of the fluxoid as the propagation on the discrete Josephson transmission line.[4,11] The network inductance L and the effective inductance of the Josephson junction can cause the small oscillation, and in this case the Josephson effective inductance is the main part of it. The small oscillations can be suppressed by increasing the value of loss term Γ. Next we set the initial condition, since the center of isolated fluxoid is the same position of Fig. 13(a), but $\gamma_y(i=1\sim15,15)=\gamma_x(15,j=1\sim15)=0.5$, and another $\gamma=0$. The

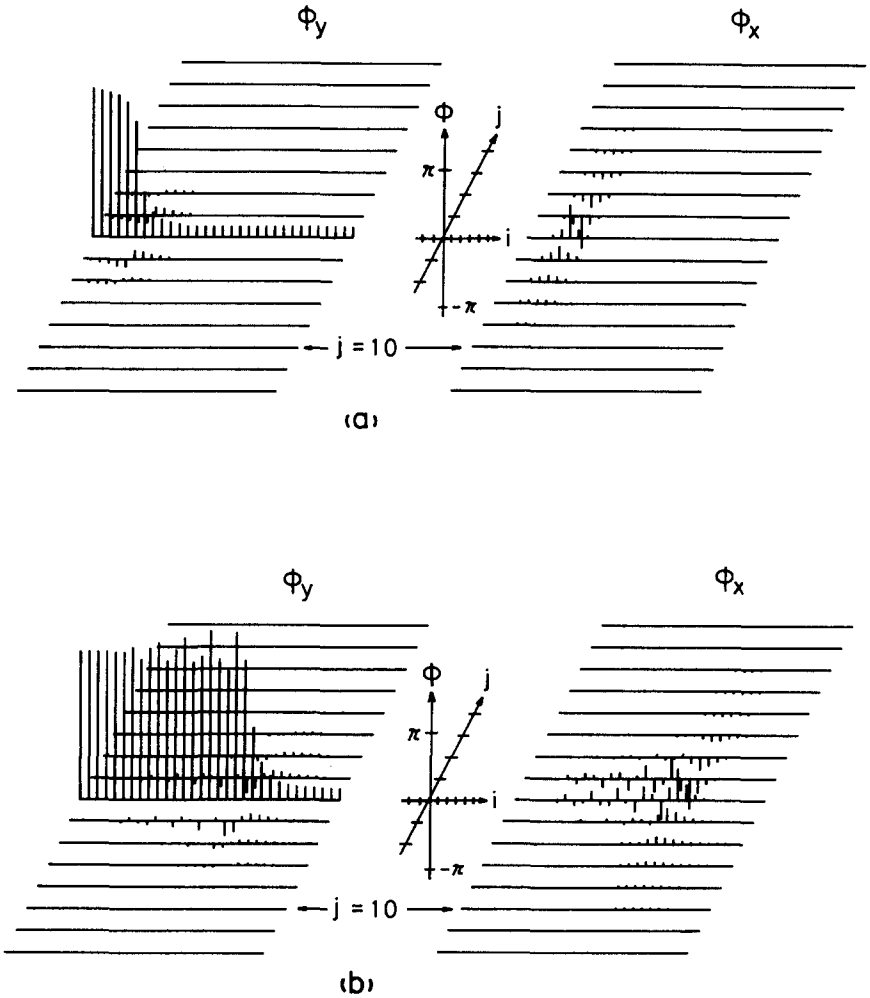

FIG. 13. Active propagation of a single fluxoid. (a) Initial value of phase parameter for the numerical calculation, where γ_y ($j=1 \sim 31$, $15)=0.5$, and another $\gamma=0$. (b) Result after 1000 times numerical iteration.

result after 1000 times numerical iteration is shown in Fig. 14(a). The fluxoid turns to right at the section $\phi_x(15,15)$ after the propagation in the direction to the right, and propagates down toward the down-side edge of the network. Since the propagation direction of the fluxoid can thus be controlled by the external applied current as in Fig. 14(a), this network is considered to be useful for the construction of logic functions. Finally we arrange the current condition such that the isolated fluxoid propagates down diagonally in a zigzag path in which one step corresponds to the one section in the network, that is $\gamma_x(31-i,i)=\gamma_y(31-i,i)=0.5$, where $i=1 \sim 30$, and other $\gamma=0$. The result after 2000 times numerical iteration is shown in Fig. 14(b), where the center of the fluxoid reaches between $\phi_y(16,15)$ and $\phi_y(17,15)$, and between $\phi_x(16,15)$ and $\phi_x(16,16)$. It was set initially between $\phi_y(6,25)$ and $\phi_y(7,25)$, and between $\phi_x(6,25)$ and $\phi_x(6,26)$. The fluxoid propagated down on the diagonal line of the square network in the downward direction. Figure 15 shows the propagating velocity of a single fluxoid as a function of γ for two external current conditions. The one external current condition corresponds to Fig. 13, and another condition corresponds to Fig. 14(b), as the inset in Fig. 15 shows. The cross symbol in the figure shows that the fluxoid cannot propagate because of a too-small bias current. The triangle symbol in the figure shows that a succession of fluxoid-antifluxoid pairs are spewed out (created) behind the initial fluxoid[11] at that value of γ. The velocity in the figure which is normalized by $u_0=1/(LC)^{1/2}$ is very small compared with u_0 which is considered to be the limiting velocity of the discrete Josephson transmission line.[4] This is due to the effective inductance of the Josephson junction. If in the case of Fig. 13 the two Josephson junctions out of four, of which the one section of the network consists, are treated as linear inductance $L_J=\hbar/2eI_c$, then we regard a section of the network as a section of the discrete Josephson transmission line and L in u_0 may be replaced by the following L',

$$L'=L+2L_J=L(1+2/HL)\ . \tag{19}$$

In the case of Fig. 15, $HL=0.1$, so

$$1/(L'C)^{1/2}=1/[LC(1+2/HL)]^{1/2}\simeq 0.22\,u_0\ . \tag{20}$$

We may adopt Eq. (20) as the limiting velocity of the square network. Upon the propagation in the direction of the x axis, if we apply the bias current of y component to all planes of the network, namely $\gamma_y(i=1 \sim 31$, $j=1 \sim 30)=0.5$, $\gamma_x=0$ (different from the case of Fig. 13), the velocity of a fluxoid is about 94% of that in the case of Fig. 13. The reason for that is considered to

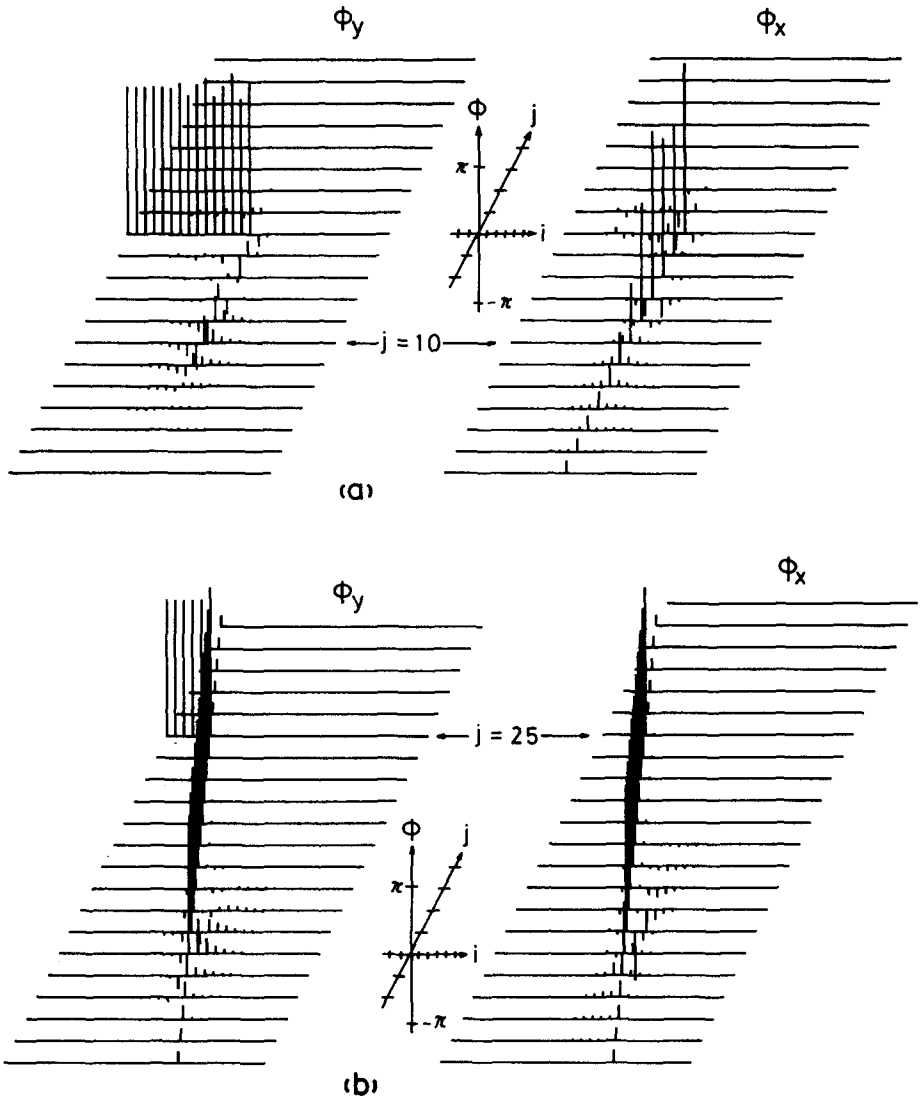

FIG. 14. Active propagation of a single fluxoid. (a) Result after 1000 times numerical iteration under the condition of γ_y ($i=1 \sim 15$, 15) $=\gamma_x$ (15, $j=1 \sim 15$) $=0.5$, and another $\gamma=0$. (b) Result after 2000 times numerical iteration where the fluxoid propagates down diagonally in a zigzag path in which one step corresponds to the one section in the network, that is γ_x ($31-i$, i) $=\gamma_y$ ($31-i$, i) $=0.5$ where $i=1 \sim 30$, and another $\gamma=0$.

be that all phases of the junctions oscillate easily because of the bias currents, so small oscillations occur with the propagation of a fluxoid, and then the small oscillations disturb the propagation of a fluxoid. The definition of velocity in Fig. 15 is the section number per unit time τ_J through which a fluxoid passes. Therefore the usual velocity is given by multiplying it by Δl which is the section length, and if a fluxoid passes obliquely through one section, it is given by multiplying by $\sqrt{2}\,\Delta l/2$. If within a unit time a fluxoid passes straight through n sections, and it passes obliquely through m sections, the usual velocity is given by multiplying by $\Delta l(n+\sqrt{2}\,m/2)$. In Fig. 15 $m=0$ for the case of straight propagation, while $n=0$ for the case of step-like propagation. The difference in the $u/u_0-\gamma$ characteristics between the straight propagation and the step-like propagation seems to be due to the different nonlinearities involved in the two routes of propagation, but the detailed study is a future subject.

Performance of the circuit is composed of two factors, (we discuss one-dimensional arrays with two- and M-junctions in a separate section ($M>4$) for simplicity). (1) Maximum information density (M.I.D.) $=N/m$ (m^{-1}), (2) Information processing speed (I.P.S.) $=n/m$ (s^{-1}),

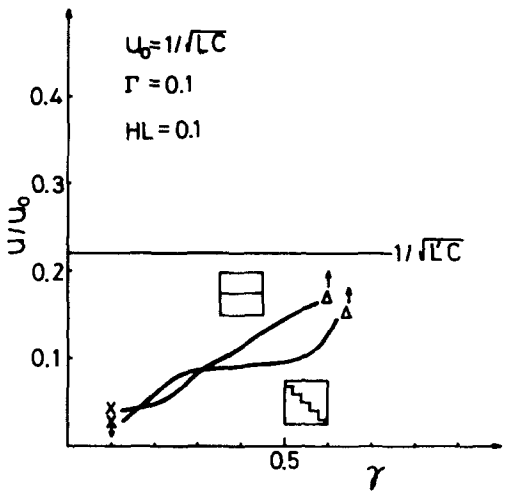

FIG. 15. Propagating velocity of a single fluxoid as a function of γ for two external-current conditions. The one external-current condition corresponds to Fig. 13, and another condition corresponds to Fig. 14(b), as the insets show. The cross symbol shows that the fluxoid cannot propagate because of a too-small bias current. The triangle symbol shows that a succession of fluxoid-antifluxoid pairs are spewed out (created) behind the initial fluxoid.

TABLE I. Comparison of performance between 2- and 4-junction cases.

	2-junction case	M-junction case
N	N	N
m	$5N\lambda_J$	2
n	$1/(LC)^{1/2}$	$\sim 1/(LC)^{1/2}$ $(M-2)^{1/2}\ N\lambda_J$
M. I. D. $=N/m$ (meter^{-1})	$1/5\lambda_J$	$N/2$
I. P. S. $=n/m$ (sec^{-1})	$1/(L_0\,C_0)^{1/2}\ 5\lambda_J$	$\sim 1/(L_0\,C_0)^{1/2}$ $2\,(M-2)^{1/2}\ \lambda_J$
I. P. E. $=nN/m^2$ (sec^{-1} meter^{-1})	$1/(L_0\,C_0)^{1/2}\ 25\lambda_J^2$	$\sim N/(L_0\,C_0)^{1/2}$ $4\,(M-2)^{1/2}\ \lambda_J$

where $N \equiv$ section number/meter, $m \equiv$ section number which one fluxoid occupies, $n \equiv$ section number which one fluxoid sweeps per unit time. One can increase N by making a small-size Josephson circuit. If one section of the circuit includes only two junctions (two-junction case), $m \cong 5N\lambda_J$, because one fluxoid occupies nearly $5\lambda_J$ (Ref. 9) where λ_J is the Josephson penetration depth. Therefore M. I. D. $(N/m) = N/5N\lambda_J = 1/5\lambda_J$ is constant in the two-junction case. If one section of the circuit includes more than four junctions (M-junction case), m is nearly equal to two independent of N (see Fig. 8). Therefore M. I. D. $(N/m) = N/2$ increases with increasing N in the M-junction case. In the 2-junction case n is represented by $\sim 1/(LC)^{1/2}$; however in the M-junction case the propagating speed of fluxoids is decreased by the kinetic inductance of additional junctions, and n is represented by $\sim 1/[LC(1+(M-2)N^2\lambda_J^2)]^{1/2}$ from Eq. (20) $(N = 1/(HL)^{1/2}\lambda_J)$. As a result, for the 2-junction case I. P. S. $(n/m) = 1/5(LC)^{1/2}N\lambda_J = 1/5(L_0C_0)^{1/2}\lambda_J$ remains independent of N, where $L_0 = LN$ and $C_0 = CN$ are the inductance and capacitance per unit length. While for the M junction case I. P. S. $(n/m) = 1/2[(M-2) + N^{-2}\lambda_J^{-2}]^{1/2}(LC)^{1/2} \times N\lambda_J \cong 1/2(M-2)^{1/2}(L_0C_0)^{1/2}\lambda_J$, so I. P. S. also remains independent of N. Furthermore, I. P. S. for the 2-junction case and for the 4-junction case is nearly equal, because the decrement of n created by inserting two additional junctions is compensated for by the decrement of m. Now we define "information processing efficiency per unit length (I. P. E.)" by the product of M. I. D. and I. P. S., which is inversely proportional to the power dissipation of the computer elements per unit length. The above observation was summarized in Table I. Therefore one can conclude that the small-size junction circuit with four junctions improves M. I. D. (N/m) and I. P. E. (nN/m^2) by a factor of N and leaves I. P. S. (n/m) unchanged.

IV. CONCLUSIONS

We derived a field equation which described two- and three-dimensional arrays of small-area Josephson junctions. The phase parameter ϕ of Josephson junctions is treated as a vector in the field equation. The field equation is reduced to the sine-Gordon equation with loss term in the one-dimensional case under the condition of $\Delta x \to 0$. And we described an equivalent circuit of the two-dimensional array of Josephson junctions based on the field equation. Next we analyzed the two-dimensional Josephson square network by using the field equation. Our model of the square network is constructed of a two-dimensional array of 31×31 superconductors. The results of our numerical calculations, which were carried out using the digital computer in the computer center of Tohoku University, are the following:

(1) When the external magnetic field is applied, the network transits to the Meissner state or the mixed state depending on the magnitude of external field. And pinning forces act on fluxoids inside the network.

(2) The field equation has a stable one-solitary solution under the free-boundary condition, that is, a single fluxoid exists stably in the network without external field. The solution can be translated to the value of the order parameter's phase which is nearly equal to the value of the angular axis when the origin of the polar coordinate is fixed at the center of the fluxoid. And the solution is not sensitive to the value of inductance, because of the effective inductance of Josephson junction.

(3) There are repulsive interactions between two fluxoids with the same sign, and there are attractive interactions between fluxoid and antifluxoid.

(4) The propagation velocity and direction of a fluxoid can be controlled by the external bias current. And the limiting velocity of fluxoid has to be modified considering the effective inductance of Josephson junction.

These results suggest a potential application of the network to high-performance computer circuits. In the simulation of the present paper we control the propagating direction of a fluxoid by the external current, but it is considered that the propagating direction can be also controlled by the external local magnetic fields. These detail studies, the investigation of a solitary solution in the three-dimensional case, and the fabrication of the real square network are the future subjects.

ACKNOWLEDGMENTS

We dedicate this paper to the memory of Professor Y. Onodera who had constantly been the leader of our group, and passed away in the course of pursuing his research in the field of superconductor devices. The authors are grateful to Professor T. Anayama, Dr. G. Ohya, and H. Tamayama for helpful discussions.

APPENDIX: COMPARISON BETWEEN THE JOSEPHSON SQUARE NETWORK AND TYPE-II SUPERCONDUCTORS

From Eqs. (2) and (17) under the condition of $\Delta l \to 0$, magnetic flux density can be written in the following form:

$$\mathbf{B} = -(\hbar/2e)(\Delta l/S)\nabla\times\Phi = \nabla\times(-\hbar/2e)(\Phi/\Delta l)\ . \quad \text{(A1)}$$

Φ may be written in the following form:

$$[\nabla\theta - (2e/\hbar)\mathbf{A}]\Delta l\ , \quad \text{(A2)}$$

because

$$\phi_x = \theta_+ - \theta_- - \frac{2e}{\hbar}\int_-^+ A_x\,dx\ , \quad \text{(A3)}$$

and so on. Therefore Eq. (A1) is reduced to the following usual relation,

$$\mathbf{B}=\nabla\times[\mathbf{A}-(\hbar/2e)\nabla\theta]=\nabla\times\mathbf{A}\ . \tag{A4}$$

If we put $\mathbf{K}=\mathbf{A}-(\hbar/2e)\nabla\theta$ under the condition of $\Delta l\to 0$, Eq. (5) is equivalent to the following equations,

$$\nabla\times\nabla\times\mathbf{K}+\mu\epsilon\partial^2\mathbf{K}/\partial t^2+\mu\sigma\partial\mathbf{K}/\partial t=\mu\mathbf{J}_s\ , \tag{A5}$$

$$\mathbf{J}_s=-J_c\sin(2e/\hbar)\mathbf{K}\Delta l\ . \tag{A6}$$

In the square network superconductors are weakly coupled to each other, therefore $(2e/\hbar)\mathbf{K}\Delta l$ in Eq. (A6) can be larger than unity. While, a type-II superconductor is not in a weak coupling state, even though we assume it to be discrete considering hypothetical lattice points. If $(2e/\hbar)\mathbf{K}\Delta l\ll 1$, and if $J_c\Delta l=(e\hbar/m)|\Psi|^2$ in Eq. (A6), where m is the mass of electron and Ψ is the order parameter, Eq. (A5) is equivalent to the London equation.[12] And in this case no mixed state is realized. In order to represent a mixed state, but different from the Josephson network, one should take the space dependence of the absolute value of order parameter into consideration unlike the square Josephson network, where it is assumed that the superconductors are larger than $2\lambda_L$, and the absolute value of order parameter is constant. The space dependence of the order parameter can be represented by using the Ginzburg-Landau equation.[13] In a Ginzburg-Landau field no pinning forces exist without defects or nonuniformity. But pinning forces exist in the square network depending upon the discreteness of network and the nonlinearity of sine function. Owing to the discreteness, it is possible to control the vortex propagation and the vortex interaction in the network and it is also possible to exchange the circuit elements as is shown in the equivalent circuit. These characteristics are important for the application of the network. The full treatment of the Ginzburg-Landau equation and Maxwell equation is more complex. We have numerically analyzed the vortex interactions based on the time-dependent Ginzburg-Landau equation in a preceding paper,[14] where we neglected the vector potential. The time-dependent Ginzburg-Landau equation is a kind of diffusion equation, so it is considered from our preceding paper that vortex-antivortex interaction always brings about the annihilation of vortices. But in the case of the square network it can be expected under the low-loss condition that vortex-antivortex interaction brings about a soliton-like behavior, namely passing through each other, because the network vortex has no normal core in the center of it.

[1] T. Van Duzer, IEEE Trans. Microwave Theory Tech. **MTT-28**, 490 (1980).
[2] S. Basavaiah, J. H. Greiner, H. H. Zappe, and S. J. Singer, J. Appl. Phys. **51**, 1702 (1980).
[3] K. Nakajima, Y. Onodera, and Y. Ogawa, J. Appl. Phys. **47**, 1620 (1976).
[4] K. Nakajima and Y. Onodera, J. Appl. Phys. **49**, 2958 (1978).
[5] T. A. Fulton and L. N. Dunkleberger, Appl. Phys. Lett. **22**, 232 (1973).
[6] T. V. Rajeevakumar, IEEE Trans. Magn. **MAG-17**, 591 (1981).
[7] T. Yamashita, Y. Ogawa, and Y. Onodera, J. Appl. Phys. **50**, 3547 (1979).
[8] T. D. Clark and P. E. Lindelof, Appl. Phys. Lett. **29**, 751 (1976).
[9] D. J. Scalapino, *Tunneling Phenomena in Solids* (Plenum, New York, 1969), p. 477.
[10] B. D. Josephson, Adv. Phys. **14**, 419 (1965).
[11] K. Nakajima, Y. Onodera, T. Nakamura, and R. Saro, J. Appl. Phys. **45**, 4095 (1974).
[12] F. London, *Superfluids* (Wiley, New York, 1950).
[13] V. L. Ginzburg and L. D. Landau, Zh. Eksp. Teor. Fiz. **20**, 1064 (1950).
[14] K. Nakajima, Y. Sawada, and Y. Onodera, Phys. Rev. B **17**, 170 (1978).